Supplementary Information

A Neurostimulant *para*-Chloroamphetamine Inhibits the Arginylation Branch of the N-end Rule Pathway

Yanxialei Jiang, Won Hoon Choi, Jung Hoon Lee, Dong Hoon Han, Ji Hyeon Kim, Young-Shin Jung, Se Hyun Kim, and Min Jae Lee

SUPPLEMENTARY FIGURE LEGENDS

Supplementary Fig. S1. Chemical Structures of *para*-methoxymethamphetamine (PMMA), *para*-methoxyamphetamine (PMA), and *para*-methylthioamphetamine (PMTA), which have identical phenylisopropylamine backbones as PCA.

Supplementary Fig. S2. (A) *In silico* docking analysis between small-molecule inhibitors and the ClpS domain (PBD code: 3DNJ). The chemical structures, binding affinities (Docking, kcal/mol), dissociation constants (K_d, μM), and calculated binding modes are shown. A protonated free amino group at the N-terminal residue appears to be essential for the interaction. However, a second residue was identified to be not critical for the inhibitory function. These data complement Fig. 1E. (B) Same as in (A) except that the effect of N-terminal acetylation and the core amide bond on the binding affinities between the ClpS domain and Phe-Ala type 2 dipeptides were calculated.

Supplementary Fig. S3.. *In silico* docking analysis between small-molecules and the UBR

box from UBR2 (PBD code: 3NY3). The binding affinities (Docking, kcal/mol) and dissociation constants (K_d, μM) are shown. (A) The N-end rule pathway was highly stereospecific such that Arg-Ala dipeptides with D-conformations had little inhibitory effects while L-Arg-Ala showed stronger interaction with the UBR box than PCA. (B) PCA showed stronger binding affinity and smaller dissociation constants than its derivatives both in the ClpS interaction and UBR box interaction. UBR2 box indicates the UBR box retrieved from UBR2. These data complement Fig. 1F.

Supplementary Fig. S4. HEK293-derived stable cell lines expressing Arg/N-end rule model substrates or the control. Similar to the *in vitro* system (Fig. 1A), Met-GFP, generated from Ub-Met-GFP, was long-lived, while Arg- and Phe-GFP proteins were rapidly degraded through the proteasome. Treatment of cells with 10 μM MG132 for 4 hr increased levels of Arg- and Phe-GFP to the comparable levels of Met-GFP. No additive or synergistic effects were observed when 1 μM of PS341 were added with 10 μM MG132.

Supplementary Fig. S5. PCA does not affect endogenous levels of RGS4 in *ATE1*$^{-/-}$ MEFs. In *ATE1*$^{-/-}$ MEFs, unlike +/+ MEFs, RGS4 proteins were long-lived and the levels of endogenous RGS4 were not changed by PCA (0, 50, 100, 200, 500 μM) treatment. These data complement Fig. 3F and 3G.

Supplementary Fig. S6. The Arg/N-end rule pathway is highly active in the brain and the neural tube. (**A**) When monitored by β-galactosidase activity, the LacZ reporter gene integrated into the targeted ATE1 allele was prominently expressed in the brain and the neural tube in embryos before E.13.5. (**B**) Histological sections with X-gal staining indicated

strong expression of ATE1 in the neural tube.

Supplementary Fig. S7. *ATE1* homozygous mutant mouse brains at E13.5 and E14.5 showed strikingly elevated levels of RGS4 compared to wild-type littermates. *ATE1*$^{+/-}$ heterozygous mice, which were virtually identical to wild-type mice in terms of gross morphology, showed no effects on RGS4 levels, indicating the haplosufficiency of ATE1 on RGS4 degradation. These data complement Fig. 5B.

Supplementary Fig. S8. Total RNA from the frontal cortex (A) and the hippocampus (B) was subjected to microarray, identifying PCA-target genes which are downregulated. PCA was intraperitoneally injected at 10 mg/kg and 20 mg/kg dose once per day for three days while saline was used as control. Mice were sacrificed 6 hr after the third PCA injection, and brains were extracted to prepare protein or mRNA samples. Gene ontology analysis was performed using DAVID. Fold changes are log base 2. $P < 0.005$. (C) Quantitative RT-PCR was performed using primers for indicated genes and GAPDH (control for normalization). The values plotted are means of three independent experiments. A value of $P < 0.05$ was accepted as statistically significant. *, $P < 0.05$. **, $P < 0.01$.

Supplementary Fig. 1

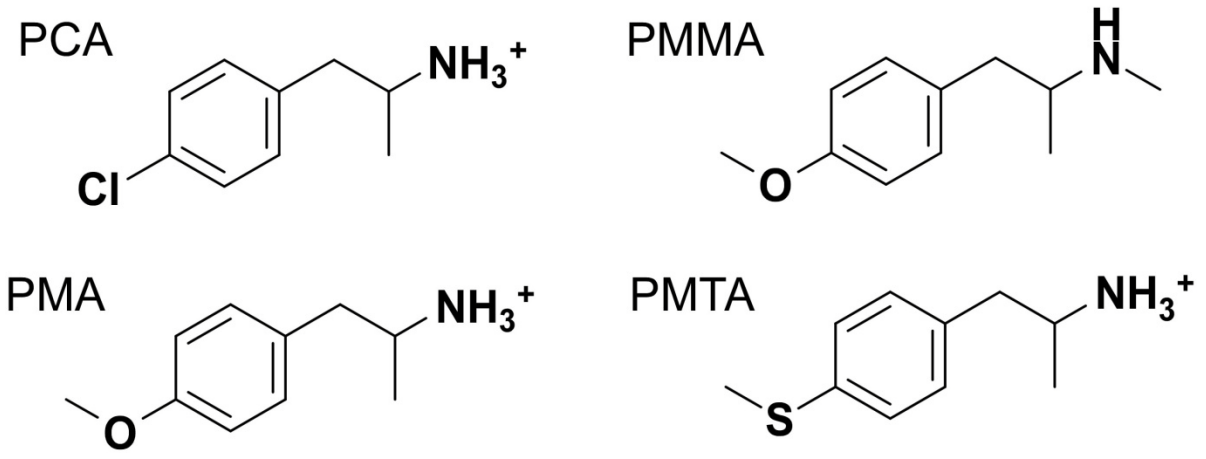

Supplementary Fig. 2

A

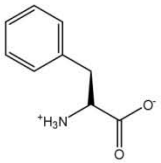

H-Phe-OH

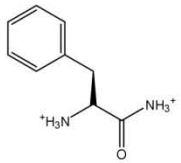

H-Phe-NH_2

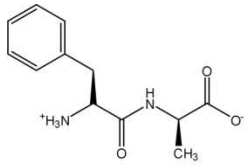

H-Phe-Ala-OH

Peptides	Docking	K_d, docking
H-Phe-NH_2	-5.37	115.71
H-Phe-OH	-3.90	1183.5
H-Phe-Ala-OH	-5.18	159.47

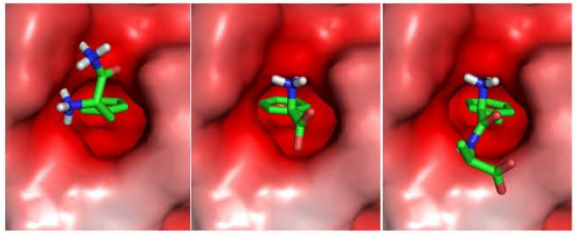

B

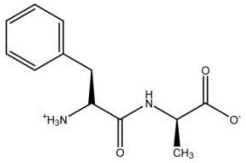

H-Phe-Ala-OH

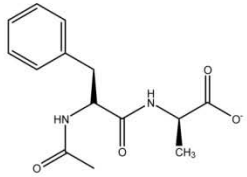

Ac-Phe-Ala-OH

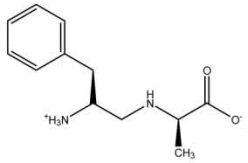

H-Phe-psi(CH_2NH)-Ala-OH

Peptides	Docking	K_d, docking
H-Phe-Ala-OH	-5.18	159.47
Ac-Phe-Ala-OH	-4.86	273.67
H-Phe-psi(CH_2NH)-Ala-OH	-4.48	519.76

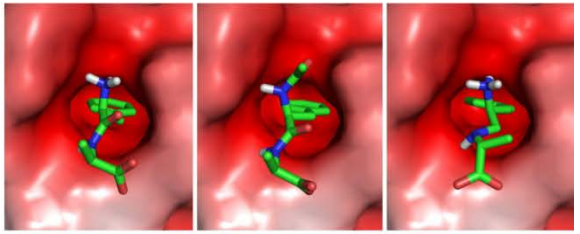

Supplementary Fig. 3

A

Peptides	docking	K_d, docking
L-Arg-Ala-OH	-8.03	0.24
D-Arg-Ala-OH	-6.27	28.50
PCA	-7.17	5.54

B

	UBR2 box	
Compound	docking	K_d, docking
PCA	-7.17	5.54
PMMA	-6.22	27.56
PMA	-6.24	26.64
PMTA	-6.21	28.03

Supplementary Fig. 4

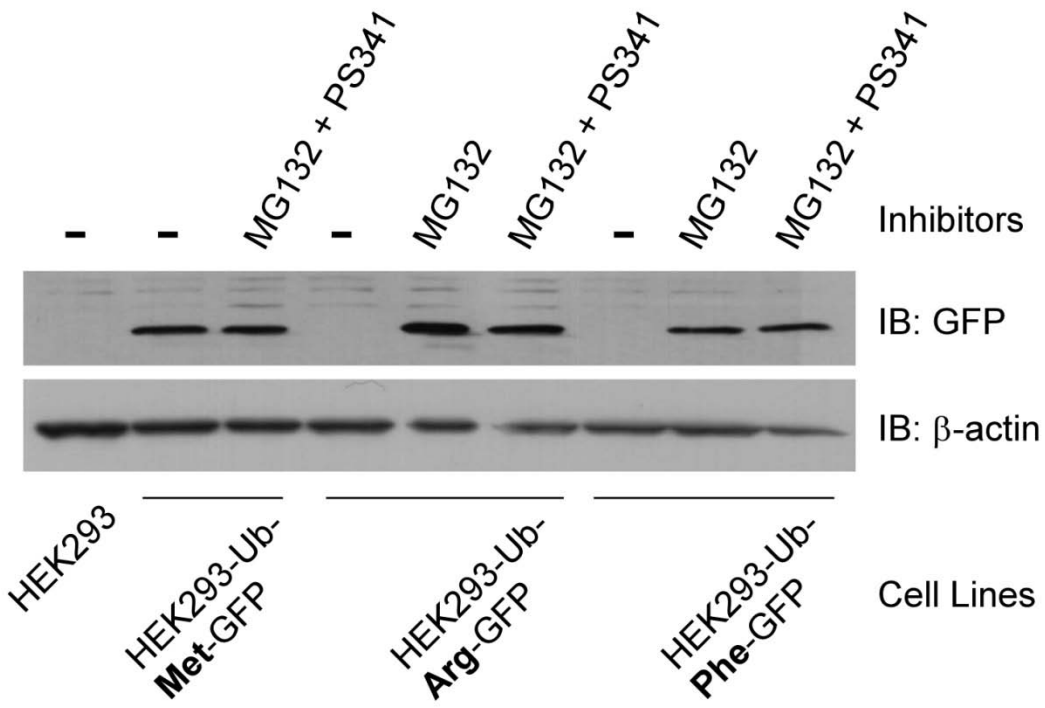

Supplementary Fig. 5

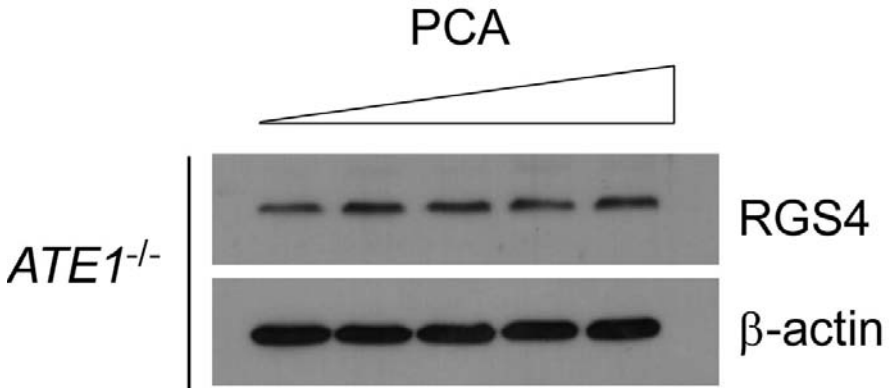

Supplementary Fig. 6

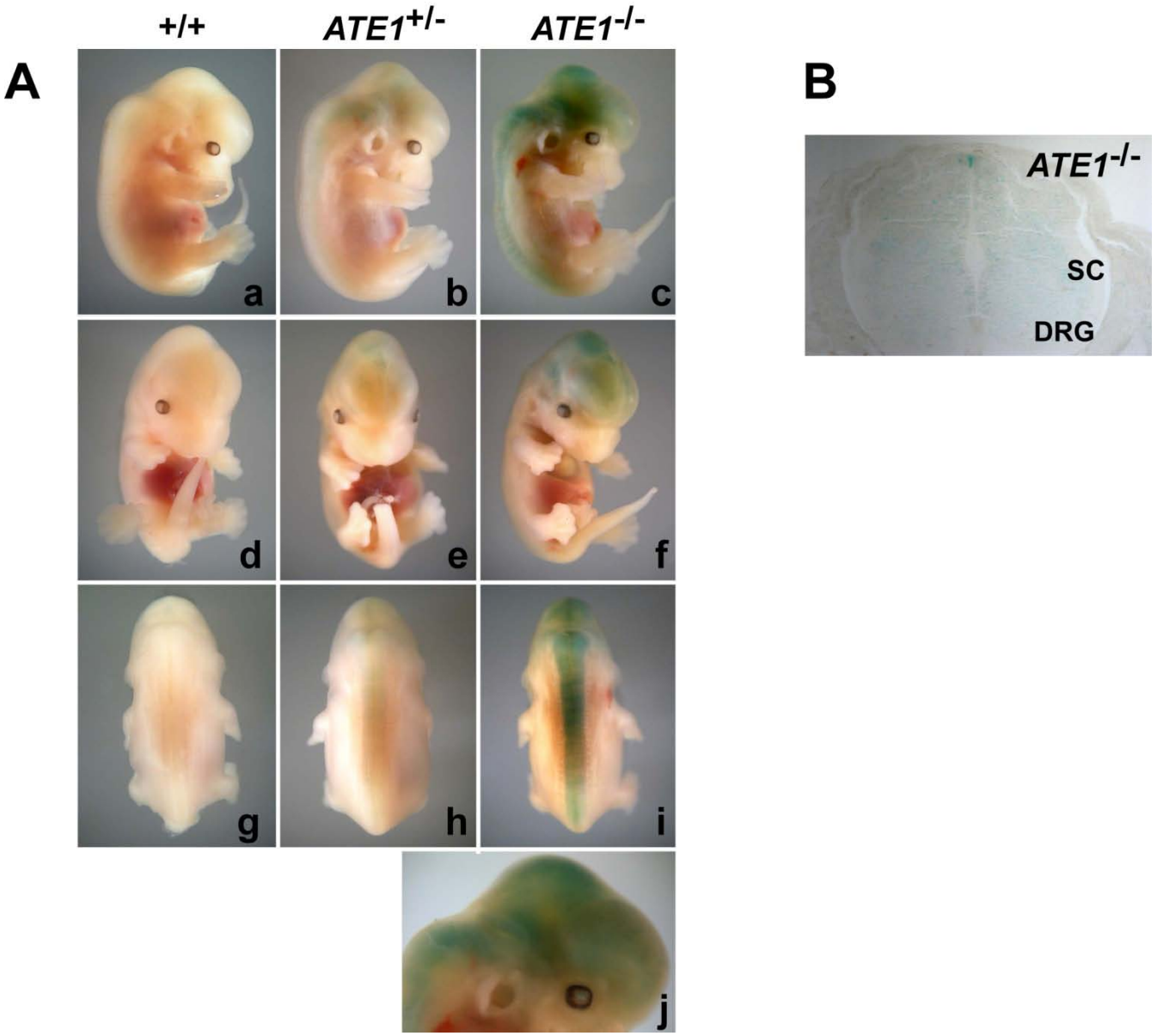

Supplementary Fig. 7

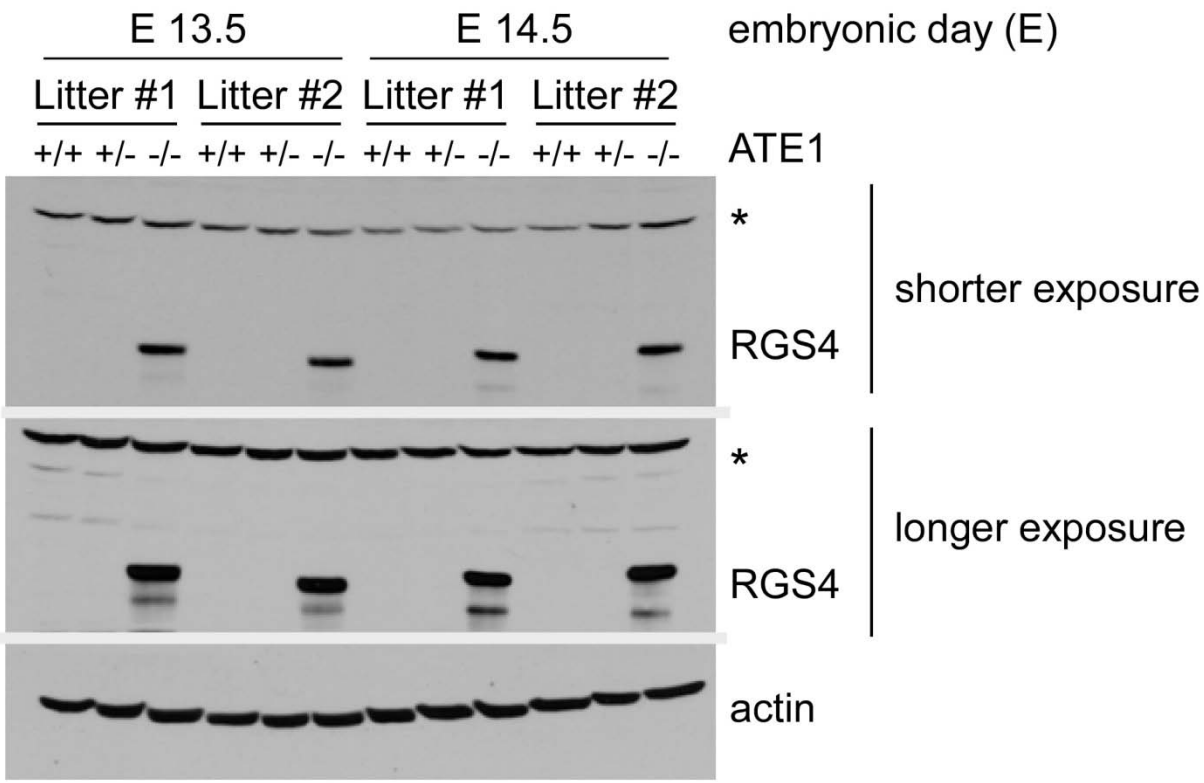

Supplementary Fig. 8A

A Frontal Cortex

Gene	Fold Inductions	Functions
Pvrl3	0.67	membrane, cell adhesion, signal peptide
Agpat3	0.66	membrane
Rassf3	0.66	cytoskeleton
Nme2	0.65	nucleotide-binding, membrane, regulation of apoptosis/proliferation
Sfrs5	0.65	regulation of transcription
Cirbp	0.65	nucleotide binding
Ly86	0.63	signal peptide
Stmn4	0.63	undefined
Cxx1c	0.63	undefined
Hes5	0.62	regulation of transcription, cell adhesion, neuron differentiation
Ggt7	0.61	membrane
Def8	0.61	metal ion-binding
Zfp316	0.61	regulation of transcription, metal ion-binding
Zc3h13	0.59	metal ion-binding
C1ql2	0.51	signal peptide
LOC100043257	0.45	undefined

B Hippocampus

Gene	Fold Inductions	Functions
Zic3	0.67	regulation of transcription, metal ion-binding
Eef2	0.66	nucleotide-binding
Rapgef4	0.66	small GTPase mediated signal transduction
Rasgrp1	0.66	small GTPase mediated signal transduction, metal ion-binding
Mapk1	0.66	kinase, regulation of transcription, vascular smooth muscle contraction
Mtch1	0.66	membrane, transport
Kl	0.66	membrane, signal peptide
Gm129	0.65	undefined
Ppp1cb	0.65	vascular smooth muscle contraction, metal ion-binding
Sumo3	0.65	ubl conjugation
Zic4	0.65	transcription factor, metal ion-binding
Eef2	0.65	nucleotide-binding
Slc6a15	0.65	transport
Gdi1	0.65	small GTPase mediated signal transduction
Prkcd	0.65	kinase, regulation of transcription, vascular smooth muscle contraction
Atp6ap2	0.65	signal peptide, membrane
Mog	0.64	signal peptide, membrane
Pfkp	0.64	nucleotide-binding, metal-binding
Necap1	0.64	transport
Ctsa	0.64	signal peptide
Ppp1cb	0.64	metal ion-binding, vascular smooth muscle contraction
Avpr1a	0.64	vascular smooth muscle contraction, chemical homeostasis
Zfp316	0.64	regulation of transcription, metal ion-binding
Sh3gl2	0.64	membrane
Hnrnpk	0.64	DNA-binding, ubl conjugation
Npas4	0.63	regulation of transcription
Mbp	0.63	chemical homeostasis
Calml4	0.63	metal ion-binding
Rbbp7	0.63	regulation of transcription
Vat1l	0.62	metal ion-binding
Pnpo	0.62	nucleotide-binding
Sfrs5	0.61	regulation of transcription
Erdr1	0.61	undefined
Sulf1	0.61	metal ion-binding, signal peptide
Cplx2	0.61	transport
Slc4a2	0.61	transport
Egr4	0.61	regulation of transcription
Atp6ap2	0.60	signal peptide
Fos	0.60	regulation of transcription
Clic6	0.60	transport
Trpm3	0.59	transport
Hspa8	0.59	vesicle, nucleotide-binding
Fus	0.58	regulation of transcription
Atp6ap2	0.58	membrane, signal peptide
Sfrs5	0.55	regulation of transcription
Otx2	0.55	regulation of transcription
Prlr	0.55	signal peptide
Egr2	0.54	regulation of transcription
Enpp2	0.53	metal ion-binding, signal peptide
Gpm6a	0.51	membrane
D830030K20Rik	0.49	undefined
Wfdc2	0.45	signal peptide
Zic1	0.43	regulation of transcription, metal ion-binding
Isl1	0.41	regulation of transcription, forebrain development
LOC100043257	0.41	undefined
1500015O10Rik	0.41	signal peptide
Zc3h13	0.41	metal ion-binding

Supplementary Fig. 8B

Supplementary Fig. 8C